International Journal of Pharmaceutics 659 (2024) 124256

Contents lists available at ScienceDirect

International Journal of Pharmaceutics

journal homepage: www.elsevier.com/locate/ijpharm

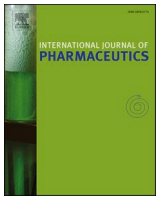

Development of inert coatings to prevent drug retention in 3D-printed diffusion cells

Carlos Bendicho-Lavilla [a,b], Victoria Díaz-Tomé [a,b,*], Iria Seoane-Viaño [a,b], Asteria M. Luzardo-Álvarez [a,b], Francisco J. Otero-Espinar [a,b,**]

[a] Department of Pharmacology, Pharmacy and Pharmaceutical Technology, Faculty of Pharmacy, and Institute of Materials (iMATUS), University of Santiago de Compostela (USC), 15782 Santiago de Compostela, Spain
[b] Paraquasil Group (GI-2109), Health Research Institute of Santiago de Compostela (IDIS), 15706 Santiago de Compostela, Spain

ARTICLE INFO

Keywords:
Stereolithography (SLA) 3D printing
Drug retention
Franz diffusion cells
In vitro release tests
Inert coatings

ABSTRACT

Diffusion cells play a crucial role in the pharmaceutical and cosmetic fields by assessing the release and permeation of active pharmaceutical ingredients across membranes. However, commercially available glass-based devices, such as Franz diffusion cells, are expensive and fragile. The emergence of three-dimensional (3D) printing technology enables the creation of diffusion cells with cost-effective polymeric materials and resins, offering exceptional precision and custom geometries. Nonetheless, there are challenges associated with interactions between 3D printing materials and drug molecules. This work aimed to develop inert coatings for 3D-printed diffusion models. Diffusion devices were designed and 3D-printed with a stereolithography (SLA) 3D printer, and different coatings were applied. Then, two model drugs were used to evaluate drug retention by coated devices. Among the tested coatings, one of them showed great potential in preventing drug retention and was selected for subsequent experiments with different drugs and conditions. Finally, voriconazole eyedrops were used to confirm the viability of 3D-printed Franz diffusion cells as a drug release diffusion model. The favourable results obtained with the coating promote the use of 3D printing as a cost-effective manufacturing technology, capable of producing diffusion cells tailored to specific study requirements.

1. Introduction

Diffusion cells are commonly used for the study of drug release and permeation of active pharmaceutical and cosmetic ingredients through polymeric or biological membranes. Pre-formulation studies include *in vitro* drug release studies (i.e., *in vitro* release tests (IVRT)) and *in vitro* permeation studies (IVPT), which are crucial for formulation development, composition optimisation and batch validation (Food and Drug Administration. FDA, 2020; Food and Drug Administration. FDA, 2022). Relevant data, such as release kinetics and drug permeation, are obtained from these studies and are essential for the characterisation of new drug formulations. *In vitro* studies are also needed to predict the *in vivo* performance of a dosage form prior to *in vivo* studies and subsequently to establish *in vitro-in vivo* correlations (IVIVC). These correlations describe the relationship between the *in vitro* properties of the dosage form (e.g., eye drops or transdermal skin formulations) and the *in vivo* response (Malinowski et al., 1997; Ghosh et al., 2015). Moreover, IVRT performed during pre-formulation development allow to discard formulations that do not meet optimal drug release requirements, thereby saving time and reducing costs. More importantly, properly conducted IVRT and IVPT allow to reduce the number of animals needed to test new formulations in future *in vivo* studies, helping to comply with the 3Rs principle in animal experimentation (Seoane-Viaño et al., 2019; NC3Rs. [cited 2023 Mar 2]. Available from: https://nc3rs.org.uk/who-we-are/3rs).

The most commonly used devices for testing drug release, diffusion and penetration of drugs across biological and synthetic membranes are glass Franz cells and Side-Bi-Side cells (Diffusion Cell Basics; PermeGear). Franz and Side-Bi-Side cells primarily consist of a donor part (donor chamber) and a recipient part (receptor chamber), which are

* Corresponding author at: Department of Pharmacology, Pharmacy and Pharmaceutical Technology, Faculty of Pharmacy, and Institute of Materials (iMATUS), University of Santiago de Compostela (USC), 15782 Santiago de Compostela, Spain.
** Corresponding author at: Department of Pharmacology, Pharmacy and Pharmaceutical Technology, Faculty of Pharmacy, and Institute of Materials (iMATUS), University of Santiago de Compostela (USC), 15782 Santiago de Compostela, Spain.
E-mail addresses: victoria.diaz@usc.es (V. Díaz-Tomé), francisco.otero@usc.es (F.J. Otero-Espinar).

https://doi.org/10.1016/j.ijpharm.2024.124256
Received 10 March 2024; Received in revised form 13 May 2024; Accepted 20 May 2024
Available online 23 May 2024

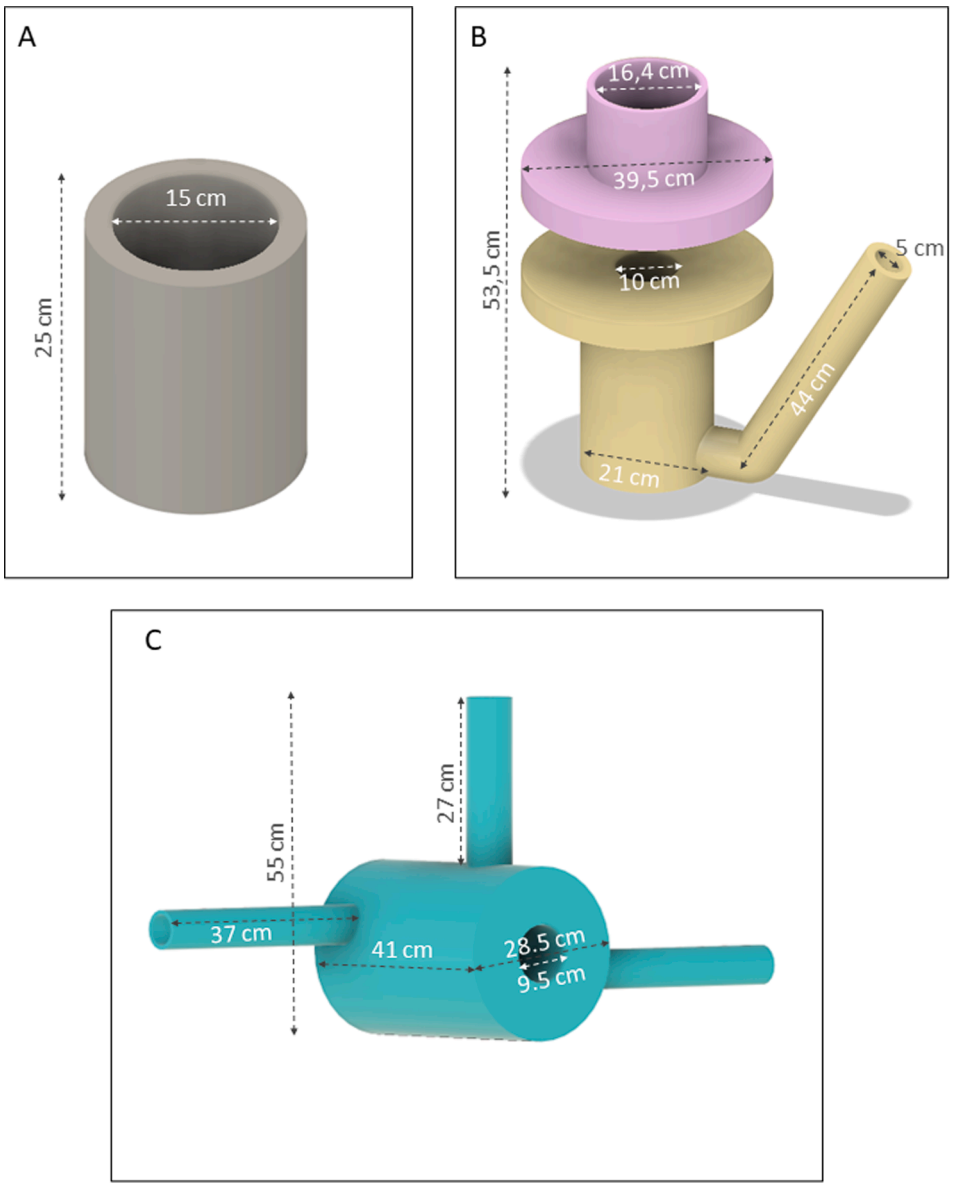

Fig. 1. (A) 3D model design of a hollow cylinder with base. (B) 3D model design of a vertical Franz diffusion cell (C) 3D model design of one of the parts of a Side-Bi-Side diffusion cell.

separated by a membrane or tissue, with a sampling port leading from the receptor chamber. A magnetic stirrer or an orbital shaker can be used to provide agitation to the medium and maintain homogeneity in both chambers. Additionally, to keep the temperature constant in the diffusion cells, a water jacket around the cell body (jacketed diffusion cells), an orbital incubator, a thermostatic bath, or a dry heating block can be employed (Diffusion Cell Basics). These static devices are used to evaluate compound uptake into or across a membrane and concentration in the receptor chamber. On the other hand, to mimic *in vivo* behaviour more closely, continuous flow cells (in-line cells) are also available. Continuous flow cells simulate blood flow, allowing to also determine the drug clearance rate (PermeGear).

Although diffusion cells are used in pharmaceutical R&D laboratories worldwide, they are not without their drawbacks (Salamanca et al., 2018; Díaz-Tomé et al., 2021). Since they are made of glass, they are very fragile and prone to breaking easily. Depending on the type and the size, its price can exceed $500 depending on the country, which makes them very expensive, especially for small laboratories and academic institutions (Fisher). In addition, different types of diffusion cells are needed based on the formulation and intended route of administration, requiring adaptation to the desired membrane or tissue type, sample volume, receptor medium, and type of agitation. For instance, some studies have focused on the development of models to mimic the physiology of the eye or the skin for *in vitro* modelling (Auel et al., 2021; Phan et al., 2021; Bown et al., 2018; Kinnunen et al., 2015). Therefore, the manufacturing of more robust, affordable and personalised diffusion cells that meet the same pharmaceutical requirements as currently commercialised glass cells is an area of ongoing development (Sil et al., 2018; Sil et al., 2020; Fazili et al., 2020; Tiboni et al., 2021).

Additive manufacturing technologies, namely three-dimensional (3D) printing, have proven to be an excellent tool for the production of spare parts and small pieces of laboratory equipment (Sil et al., 2018; Seoane-Viaño et al., 2022; Mohmmed et al., 2017). The affordability and design flexibility offered by this technology along with the wide variety of low-cost materials that can be used make 3D printers essential in any research laboratory (Seoane-Viaño et al., 2021; Anycubic Resin Printer - Anycubic. [cited 2023 Nov 18]. Available from: https://www.anycubic.es/.; Creality Resin Printer - Creality. [cited 2023 Nov 18]. Available

Table 1
Main composition of the products used as coatings.

	Main polymer	Solvents	Other components	Source/ supplier
Coating A	Plioway®	Alkanes, C14-17, chlorine,chlorinated kerosenes	Pigments and fillers	PRF
Coating B	1,1,1,2-Tetrafluoroethane	Isopropyl Alcohol	Pigments and fillers	Miller-stephenson
Coating C	Mixture of pure acrylic emulsions and self-crosslinking elastomers	Trimethoxyvinylsilane, trimethoxy(vinyl)silane, 2,2′-iminodiethanol, diethanolamine	Pigments and fillers	Cromology
Coating D	Epoxy-polyamidoamine resins (Polímero con 2,2-Bis(p-(2,3-Epoxipropoxi)Fenil) Propan)	Xylene, Hydrocarbons, C9, aromatic, 2-Methylpropan-1-ol, 2-methoxy-1-methylethyl acetate, Ethylbenzene, n-butyl acetate, Formaldehyde.	Pigments and fillers	Tkrom®
Coating E*	Bisphenol A-based epoxy resins plus aliphatic polyamine adduct	Xylene, 2-Methylpropan-1-ol,2-methoxy-1-methylethyl acetate, Ethylbenzene, n-butyl acetate, Formaldehyde, 2-methoxy-1-methylethyl acetate, A mixture of: N,N-Ethane-1,2-diylbis(decanamide)/12-Hydroxy-N-[2-[1-[1-oxydecyl) amino]ethyl]octadecanamide/N,N-Ethane-1,2-diylbis(12-hydroxyoctadecanamide	Pigments and fillers	Tkrom®
Coating F	Bisphenol A-based epoxy resins plus aliphatic polyamine adduct	Xylene, 2-Methylpropan-1-ol,2-methoxy-1-methylethyl acetate, Ethylbenzene, n-butyl acetate, Formaldehyde, 2-methoxy-1-methylethyl acetate, A mixture of: N,N-Ethane-1,2-diylbis(decanamide)/12-Hydroxy-N-[2-[1-[1-oxydecyl) amino]ethyl]octadecanamide/N,N-Ethane-1,2-diylbis(12-hydroxyoctadecanamide		Tkrom®
Coating G	Poly(Bisphenol A-co-epichlorohydrin), glycidyl end-capped	Ethyl acetate		Merk

* The composition was obtained from the Safety Data Sheet of the products.

from: https://www.creality3dofficial.com/collections/lcd-uv-resin-3d-printer.; ELEGOO Resin Printer - ELEGOO. [cited 2023 Nov 18]. Available from: https://www.elegoo.com/pages/elegoo-bf2022?gclid=Cj0KCQiA99ybBhD9ARIsALvZavXU5pZ1yPOz2g3Lb6ajr97MJ1cG6k7G_7bHAyeBqtJJf-tm-J_VqcYaArVTEALw_wcB). Among the available 3D printing technologies, stereolithography (SLA) 3D printing creates objects in a layer-by-layer fashion by selectively solidifying a liquid resin composed of monomers and a photoinitiator. This technology is highly adequate to 3D print small parts with complex geometries at very high resolutions (<10 μm) and very short times (Xu et al., 2021; Rodríguez-Pombo et al., 2022). Even more interesting, completely solid objects can be created, thus avoiding the risk of leakage when liquids are introduced inside, this being very relevant if the object to be printed are diffusion cells.

However, the main problem with this technology lies in the use of photocurable resins, mainly composed of acrylates (Voet et al., 2018). Acrylic materials are permeable to various substances, including solvents and solutes (e.g., drugs) (Bendicho-Lavilla et al., 2023). In addition, these materials can absorb water and other solvents, and depending on their degree of cross-linking, they can even exhibit swelling (Benmessaoud et al., 2020). As a result, drug surface adsorption issues may arise when in contact with a pharmaceutical formulation (Sil et al., 2018). Ideally, this problem could be solved by applying a coating that prevents the drug from adhering to the wall of the printed device. Although some research has been carried out to explore materials that can be used as inert coatings for the interior of 3D-printed objects to prevent drug retention, none of them have been successful so far (Sil et al., 2018).

The aim of this study was to develop inert coatings for 3D-printed diffusion models. Initially, a basic hollow cylinder 3D model was created using CAD software and subsequently printed using an SLA 3D printer. Subsequently, various coatings were applied to the 3D-printed hollow cylinders to assess their ability to retain two model drugs in comparison to glass vials. Among the coatings tested, one exhibited promising potential and was chosen for further experimentation with diverse drugs and model conditions. To validate the model, an *in vitro* release test was conducted on 3D-printed coated Franz cells, as well as commercially available glass Franz cells, utilising a voriconazole eye drop formulation. The selected coating was also subjected to additional characterisation, evaluating its reusability and resistance to solvents, pH, and temperature. Finally, the chosen opaque coating was compared to both a translucent coating with a similar composition and an in-house made coating based on the main polymer of the opaque and translucent coating.

2. Materials and methods

2.1. Materials

405 nm Clear UV Resin was purchased from Anycubic (Shenzhen, China), ciclopirox olamine and dexamethasone base were obtained from Acofarma (Barcelona, Spain), voriconazole was purchased from Normon (Madrid, Spain), bevacizumab (Avastin®) was purchased from Roche (Basel, Switzerland), insulin was purchased from Merck (Darmstadt, Alemania), hydroxocobalamin acetate was obtained from HealthTech BioActives (Barcelona, Spain), 2-hydroxypropyl-β-cyclodextrin (HPβCD) (Kleptose®, 0.65 M substitution ratio, MW 1399 Da) was purchased from Roquette Laisa S.A. (Valencia, Spain), and hyaluronic acid (HA) was obtained from Acofarma (Barcelona, Spain). Polytetrafluoroethylene (PTFE) powder spray coating (A), Plioway® resin-based coating (B), acrylic and self-crosslinking elastic emulsion coating (C), epoxy-polyamidoamine resin-based coating (D), bisphenol A epoxy resin-based opaque coating (E), and bisphenol A epoxy resin-based translucent coating (F) were purchased in the local hardware store. Poly(Bisphenol A-co-epichlorohydrin), glycidyl end-capped was purchased from Merck (Darmstadt, Alemania).

2.2. 3D printing process and leak testing

Two types of 3D models were designed and printed: hollow cylinders and Franz diffusion cells. The 3D hollow cylinders were used for the preliminary tests to facilitate the work, as they are easier to manipulate. The CAD software Fusion 360 V2.0.16265 (Autodesk Inc., USA) was used to design the 3D models. The 3D model of the vertical Franz cell was designed from measurements obtained with a digital Vernier calliper of a common glass vertical Franz cell. The receptor volume in both 3D-printed and glass vertical Franz cells was 6.5 mL. The resultant. stl files were sliced using the slicer software Photon Workshop V2.1.29 (Anycubic, Shenzhen, China). The printing parameters consisted of a layer height of 0.05 mm and a UV light (405 nm) exposure time of 2 sec. The final objects were printed using a Photon Mono X 6 K 3D printer (Anycubic, Shenzhen, China). The 3D printed devices were then washed

Table 2
Physicochemical properties of the model drugs.

Drug	Molecular weight (Da)*	logP (o/w)*	pKa/ Isoelectric point*	Aqueous solubility ($mg \cdot mL^{-1}$, 25 °C)*
Dexamethasone base	392.5	1.83	1.89 and 6.18	0.089 at pH 7.0
Ciclopirox olamine	268.35	2.3	6.84	1.41 at pH 7.0
Human insulin	5808	−13.1	5.4	2 at pH 2–3
Bevacizumab	149,000	–	8.3	–
Voriconazole	349.31	1.75	1.76	2.7 at pH 1.2
Hydroxocobalamin acetate	1346.35	−14	1.81	>15 at pH 7.0

* Data extracted from PubChem (PubChem. [cited 2023 Sep 22]. Available from: https://pubchem.ncbi.nlm.nih.gov/).

with isopropanol in an ultrasonic bath and cured in a UV light cabinet for 1 min on each side. Fig. 1 shows the 3D model designs of the hollow cylinder and the vertical Franz diffusion cell used for the studies.

Liquid leakage assessment was conducted by filling a batch of 3D-printed coated devices and 3D-printed coated vertical Franz diffusion cells with a predetermined volume of water and placing them at 4 °C to prevent water evaporation. At different times, the devices were weighed and visual inspected to evaluate any weight loss or presence of any external water leakage.

2.3. Selection and application of coatings

Several types of coatings were tested along with uncoated 3D-printed cylinders and glass vials. The selection of coatings was based on their potential to prevent drug retention. The following coatings were evaluated: PTFE powder spray coating (A), Plioway® resin-based coating (B), acrylic and self-crosslinking elastic emulsion coating (C), epoxy-polyamidoamine resin-based coating (D), and bisphenol A epoxy resin-based opaque coating (E). The main composition of the coatings is summarised in Table 1.

Coating A was applied by spraying the interior of the 3D-printed cylinders 5 times, with a 30-minute dry period between applications. The remaining coatings were applied by filling the inside of the 3D-printed cylinders and removing excess material 30 min later. The cylinders were left to dry for 48 h.

2.4. Preliminary screening of the coatings

The coatings were tested with two model drugs, ciclopirox olamine and dexamethasone base. A 25 μg/mL dexamethasone base solution (pH 7.25) and a 50 μg/mL ciclopirox olamine solution (pH 8.5) were prepared. The 3D-printed cylinders were coated according as described in Section 2.3 and subsequently filled with the corresponding solution, covered with Parafilm® M sealing film, and maintained at 4 °C to avoid evaporation. Drug retention was assessed in comparison to uncoated cylinders and borosilicate glass type I vials by measuring drug concentration at different time points (1, 2, 5 and 8 days) using ultra high-performance liquid chromatography (UHPLC) (ACQUITY UPLC H-Class Plus, Waters, Milford, Massachusetts, USA) with an FTN injector and PDA detector. All experiments were performed in triplicate.

For ciclopirox olamine the stationary phase was an ACQUITY UPLC BEH 1.7 μm C18 column, 2.1 × 50 mm (Waters, Massachusetts, USA), and the mobile phase was an isocratic elution of 60 % orthophosphoric acid 20 mM and 40 % acetonitrile pumped at a flow rate of 0.5 mL/min. The injection volume was 50 μL, and column temperature was set to 30 °C with UV-wavelength of 300 nm. The elution time of ciclopirox olamine was approximately 0.85 min.

For dexamethasone base the stationary phase was an ACQUITY UPLC BEH 1.7 μm C18 column, 2.1 × 50 mm (Waters, Massachusetts, USA), and the mobile phase was an isocratic elution of 65 % water 0.1 % trifluoroacetic acid (TFA) 35 % methanol pumped at a flow rate of 0.7 mL/min. The injection volume was 5 μL, and column temperature was set to 35 °C with UV- wavelength of 241 nm. The elution time of dexamethasone base was approximately 1.9 min.

Chromatograms were processed using Empower 3 software (Waters, Massachusetts, USA). Drug recovery (Eq. (1) in each time point was calculated with the following equation:

$$Drug\ recovery\ (\%) = \frac{[Drug]\ in\ the\ coated\ 3D\ printed\ cylinder}{[Drug]\ in\ the\ glass\ vial} \bullet 100 \qquad (1)$$

2.5. Preparation of formulations with selected model drugs

Coated and uncoated 3D-printed cylinders and glass vials were subjected to a preliminary drug retention test using dexamethasone base and ciclopirox olamine solutions. One of the coatings was selected for subsequent tests. To validate the chosen coating, drug model solutions were prepared, including human insulin, bevacizumab, voriconazole with 0.1 % (w/v) 2-hydroxypropyl-β-cyclodextrin (HPβCD), and hydroxocobalamin acetate. Drug selection was made based on their different physicochemical properties, which are contained in Table 2.

2.6. Drug retention studies with the selected coating

Given the positive results obtained with coating E, further drug retention studies were conducted using 100 μg/mL human insulin (pH 2.3), 25 μg/mL bevacizumab (pH 6.15), 50 μg/mL voriconazole with 0.1 % (w/v) 2-hydroxypropyl-β-cyclodextrin (HPβCD) (pH 7.12), and 50 μg/mL hydroxocobalamin acetate (pH 5.71) solutions. All experiments were performed in triplicate. Drug recovery was evaluated using various chromatographic methods, as described in Section 2.4.

For insulin the stationary phase was an ACQUITY UPLC BEH 1.7 μm C18 column, 2.1 × 50 mm (Waters, Massachusetts, USA), and the mobile phase was an isocratic elution of 65 % potassium phosphate 0.1 M pH 3.1 buffer, 27 % acetonitrile, and 8 % methanol. The flow rate was set to 0.6 mL/min, with an injection volume of 10 μL, a column temperature of 25 °C, and a UV wavelength of 214 nm. The elution time of insulin was approximately 0.98 min.

For bevacizumab the stationary phase was a BioResolve RP mAb Polyphenyl, 2.7 μm 450 Å column, 2.1 × 50 mm (Waters, Massachusetts, USA), and the mobile phase was a gradient from 15 % water 0.1 % trifluoroacetic acid (TFA) and 85 % acetonitrile 0.1 % TFA to 85 % water 0.1 % TFA and 15 % acetonitrile 0.1 % TFA. The flow rate was set to 0.8 mL/min, with an injection volume of 1 μL, a column temperature of 80 °C, and a UV wavelength of 280 nm. The elution time of bevacizumab was approximately 2.4 min.

For voriconazole the stationary phase was a ACQUITY UPLC BEH 1.7 μm C18 column, 2.1 × 50 mm (Waters, Massachusetts, USA), and the mobile phase was an isocratic elution of 70 % 10 mM ammonium acetate buffer and 30 % acetonitrile. The flow rate was set to 0.5 mL/min, with an injection volume of 10 μL, a column temperature of 25 °C, and a UV wavelength of 256 nm. The elution time of voriconazole was approximately 2 min.

For hydroxocobalamin acetate the stationary phase was a CORTECS UPLC 1.6 μm C8 column, 2.1 × 100 mm (Waters, Massachusetts, USA), and the mobile phase was an isocratic elution of 90 % 10 mM ammonium formiate and 10 % acetonitrile. The flow rate was set to 0.4 mL/min, with an injection volume of 10 μL, a column temperature of 40 °C, and a UV wavelength of 351 nm. The elution time of hydroxocobalamin acetate was approximately 0.85 min.

2.7. In vitro release study of a voriconazole eye drop in vertical glass Franz cells and 3D-printed coated Franz cells

Firstly, a voriconazole hydrogel eye drop formulation developed in a

previous study (Díaz-Tomé et al., 2021) was prepared by adding 0.4 % (w/v) hyaluronic acid to a 1 % (w/v) voriconazole solution with a 20 % (w/v) HPβCD. An *in vitro* release study was then conducted to compare the release profiles of the voriconazole eye drop formulation in 3D-printed coated vertical Franz cells and glass vertical Franz cells. 0.5 mL of formulation was added to the donor compartment, while the receptor compartment was filled in with 6 mL of phosphate-buffered saline (PBS) pH 7.4. Visking® dialysis membranes (Medicel® membranes Ltd.) with a 12–14 Kda cut-off (0.784 cm^2 available surface area) were placed between donor and receptor compartments. The Franz cells were kept thermostated at 37 °C and the medium homogenised by placing them in an orbital shaker incubator (Unimax 1010 and Inkubator 1000, Heidolph, Schwabach, Germany) at 100 rpm during the assay. Samples of 1 mL were withdrawn at pre-determined time points and replaced with fresh PBS medium. The concentration of voriconazole was determined by the method previously described in Section 2.6.

2.8. Morphological and physicochemical characterisation of the selected coating

2.8.1. Scanning electron microscopy and energy dispersive X-ray analysis

The morphological properties of the E coating surface were examined by scanning electron microscopy (SEM). SEM images of the coated and uncoated devices were taken with a ZEISS EVO LS15 microscope at 20Kv using a BSD detector (backscattered electron detector)/SE (secondary electron detector), under conditions of variable pressure.

Elemental microanalysis of the coating E was performed by energy dispersive X-ray analysis (EDX) with an EDS Ultim® Max detector (Oxford Instruments) controlled by INCA software. The acquisitions conditions were 20Kv and a working distance of 8.5 mm for a more precise analysis.

2.8.2. X-ray diffraction

X-ray diffraction (XRD) measurements were carried out using an Empyrean diffractometer (Malvern Panalytical, UK). The X-rays were obtained from a sealed tube with a Cu anode ($\lambda(K_{\alpha 1}) = 1.5406$ Å) which was collimated, prior to incidence on the sample, with an optic including a W/Se type bilayer mirror. The radiation emitted by the sample was obtained with a "PIXcel3D" type solid-state detector. The diffractograms were taken in an angular range from 2° to 40° with a step of 0.02° and a time per step of 2 sec. Phase identification of the obtained diffractograms was performed using HighScore Plus 3.0d software (Malvern Panalytical, UK).

2.8.3. Raman spectroscopy

Raman spectroscopy was performed on the coated and uncoated 3D-printed devices using a Bruker Raman FT Raman Scope. The Raman spectra provided information on the functional groups of the materials, allowing comparison of the chemical composition of coated and uncoated devices. Raman spectra were recorded at room temperature on a Raman confocal microscope alpha300 R (WITec) using a 532 nm laser with a power of 1.3–2.1 mW, 0.3 s of integration time, 50 accumulations, and a lens of 50x LD. Project Five 5.3 (WITec) was used for data processing and imaging.

2.9. Evaluation of the reusability of coated devices

The 3D-printed cylinders coated with coating E, which were used in sections 2.6 and 2.7, were cleaned with a neutral detergent or a neutral detergent and alcohol. The cylinders were then analysed using EDX, XRD, and Raman spectroscopy. The Scherrer's formula (Eq. (2) was used as a measure of the crystallinity of coating E before and after washing:

$$Dp = \frac{K \bullet \lambda}{B \bullet cos\theta} \quad (2)$$

where Dp is the average crystallite size (nm), K is the Scherrer constant (0.94 for spherical crystallites with cubic symmetry), λ is the X-ray wavelength (for mini XRD, Cu Kα = 1.541787 Å), B is the full width at half maximum (FWHM) of XRD peak and θ is the XRD peak position.

Comparisons with data from unused coated devices from Section 2.8 were made to examine whether any drug residue was retained. Subsequently, a 25 μg/mL of dexamethasone base solution was loaded into the 3D-printed coated recycled cylinders, and dexamethasone retention was assessed according to the procedure described in Section 2.4.

2.10. Solvent resistance of the selected coating

The 3D-printed cylinders coated with coating E were exposed to different solvents including acetone, ethanol, isopropanol, neutral detergent, methanol, or liquid paraffin for 24 h. After exposure to the solvents, the cylinders were dried and analysed using SEM as described in Section 2.8 to assess any potential changes in the surface morphology of the coatings. Solvents were checked visually for any turbidity after the test period and the coatings were inspected for any structural changes such as pinholes or blemishes.

2.11. Temperature and pH resistance

The resistance of the coating E to temperature was assessed by exposing the 3D-printed cylinders to different temperature conditions. Conditions tested included 4 °C, 25 °C and 37 °C. A 25 μg/mL dexamethasone base solution was added to the 3D-printed coated cylinders and drug retention was assessed following the method described in Section 2.4.

The resistance of the coating E to changes in pH was investigated by exposing the 3D-printed cylinders to neutral, acidic and basic pH buffers for 24 h. Buffers consisted of pH 7.5 and pH 9.0 phosphate buffer solution, and pH 1.2 simulated gastric fluid without enzyme (Buffer Solutions. European Pharmacopoieia, 2010.). Subsequently, the buffers were removed, and a 25 μg/mL dexamethasone base solution was added to the 3D-printed coated cylinders. Drug retention was assessed following the method described in Section 2.4.

2.12. Comparison between the opaque coating (E), the translucent coating (F), and the in-house made coating (G)

The coating G was elaborated by dissolving 10 % (p/v) poly (bisphenol A-co-epichlorohydrin), glycidyl end-capped in ethyl acetate. The coatings F and G were applied by filling the inside of the 3D-printed cylinders and removing excess material after 30 min. Subsequently, the cylinders were left to dry for 48 h. Both coatings were analysed using SEM, EDX, XRD, and Raman spectroscopy as detailed in Section 2.8.

Coating F retention was assessed by adding a 25 μg/mL dexamethasone base solution to the coated 3D-printed cylinders. Drug retention was analysed following the method described in Section 2.4.

Coating G retention was characterised in depth by adding the following solutions: 100 μg/mL human insulin, 25 μg/mL dexamethasone base, 50 μg/mL voriconazole with 0.1 % (w/v) 2-hydroxypropyl-β-cyclodextrin (HPβCD), 50 μg/mL hydroxocobalamin acetate, and 50 μg/mL ciclopirox olamine. Drug recovery was evaluated using various chromatographic methods, as described in Sections 2.4 and 2.5.

3. Results and discussion

3.1. Design, manufacture, coating, and leak testing of 3D-printed devices

For the design of the diffusion cells, the measurements of a standard glass diffusion cell were replicated to achieve a comparable internal volume. The donor and receptor chambers were 3D-printed separately and positioned upside down to eliminate the need for supports. The resulting components exhibited smooth walls without requiring

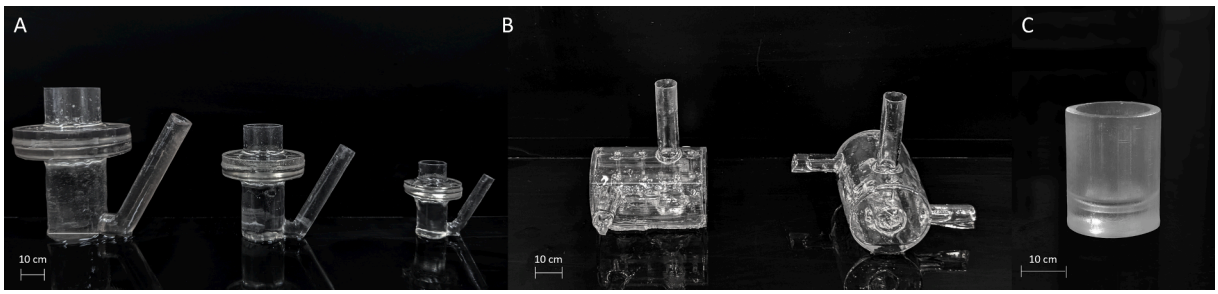

Fig. 2. (A) 3D printed vertical diffusion Franz cells in different sizes. (B) 3D printed Side-Bi-Side cell. (C) 3D printed cylinders.

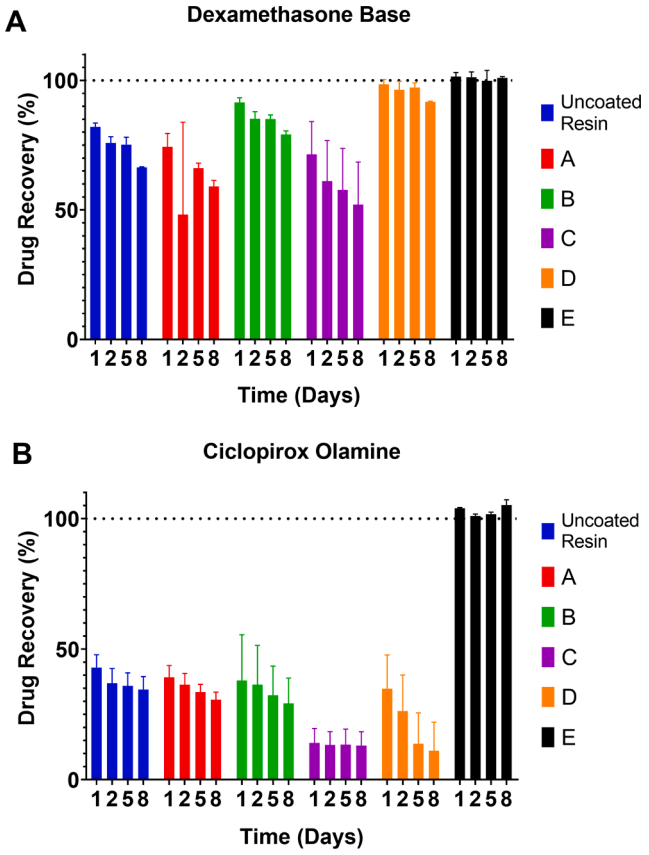

Fig. 3. Drug recovery (%) from coated and non-coated 3D printed vials compared to glass vials. (A) Dexamethasone base recovery (%). (B) Ciclopirox olamine recovery (%).

additional sanding or post-processing (Fig. 2). The chosen layer height of 0.05 mm enabled the production of 3D-printed diffusion cells with excellent resolution. In addition, the durability of the 3D-printed devices was assessed through drop and shock tests (data not shown), which demonstrated superior robustness in comparison to glass diffusion cells. To facilitate the studies, 3D printed cylindrical vials were employed for preliminary investigations.

The high level of adhesion between layers achieved through SLA printing ensures the production of watertight 3D-printed devices. The leak detection study performed on the 3D printed devices resulted in no liquid leakage observed and no significant change in the weight of the devices during the studied period (α n.s.). However, one of the challenges associated with using SLA technology for manufacturing pharmaceutical equipment lies in the utilisation of acrylic resins, which are not inert and can potentially undergo chemical or physical interactions with many drugs (Sil et al., 2018). Consequently, various coatings were selected based on their ability to prevent drug retention and were applied to the components of the devices that come into contact with the drug solution.

3.2. Preliminary screening of the coatings

An initial evaluation of the coatings was conducted through a drug retention study, involving two drugs with distinct chemical properties: dexamethasone base and ciclopirox olamine. Fig. 3 shows the results of drug recovery (%) from the preliminary test. On day 8, the uncoated resin device retained 33.58 ± 0.21 % of dexamethasone base and 65.43 ± 4.95 % of ciclopirox olamine. Similarly, the retention of dexamethasone base for coatings A, B, C and D on day 8 was 40.93 ± 2.33 %, 20.90 ± 1.41 %, 47.94 ± 16.39 %, and 8.30 ± 0.27 %, respectively. For ciclopirox olamine, the retention on day 8 was even higher, with values of 69.35 ± 2.90 %, 70.74 ± 9.65 %, 86.89 ± 5.30 %, and 88.86 ± 10.93 % for coatings A, B, C, and D, respectively. Contrarily, coating E exhibited complete recovery with no retention observed for either drug at any time point. There were no significant differences found between time points for dexamethasone base (α n.s.). However, the retention of ciclopirox olamine in the glass container increased with contact time ($\alpha < 0.05$). The recovery of ciclopirox from coating E reached approximately 105 % on day 8. Based on these promising results, coating E was further tested with drugs of different chemical properties to assess its drug retention.

3.3. Drug retention with the selected coating

Coating E was subjected to additional drug retention testing with drugs of diverse characteristics, including hydroxocobalamin acetate, voriconazole, human insulin, and bevacizumab. The latter two are biomacromolecules—a protein and a monoclonal antibody, respectively—becoming increasingly relevant for clinical applications (Bendicho-Lavilla et al., 2022; García-Otero et al., 2022). Certain studies suggest that proteinaceous molecules can bind to borosilicate glass type I containers. Therefore, one of the objectives of this study was to evaluate the potential binding to coating E (Wei et al., 2014).

Drug solutions tested included human insulin, bevacizumab, voriconazole and hydroxocobalamin acetate. Fig. 4 shows the percentage of drug recovery for each drug at different time points. No significant differences were observed between time points for hydroxocobalamin acetate, voriconazole, and insulin (α n.s.). However, in the case of bevacizumab, the retention in glass vials was higher compared to the coated devices ($\alpha < 0.05$). Extensive studies have been conducted on the retention of proteins and monoclonal antibodies in glass containers (Wei et al., 2014; Hoehne et al., 2011), and the findings of this study align with the existing literature. Consequently, coating E demonstrates the potential to prevent interactions between protein-based drugs and their primary container.

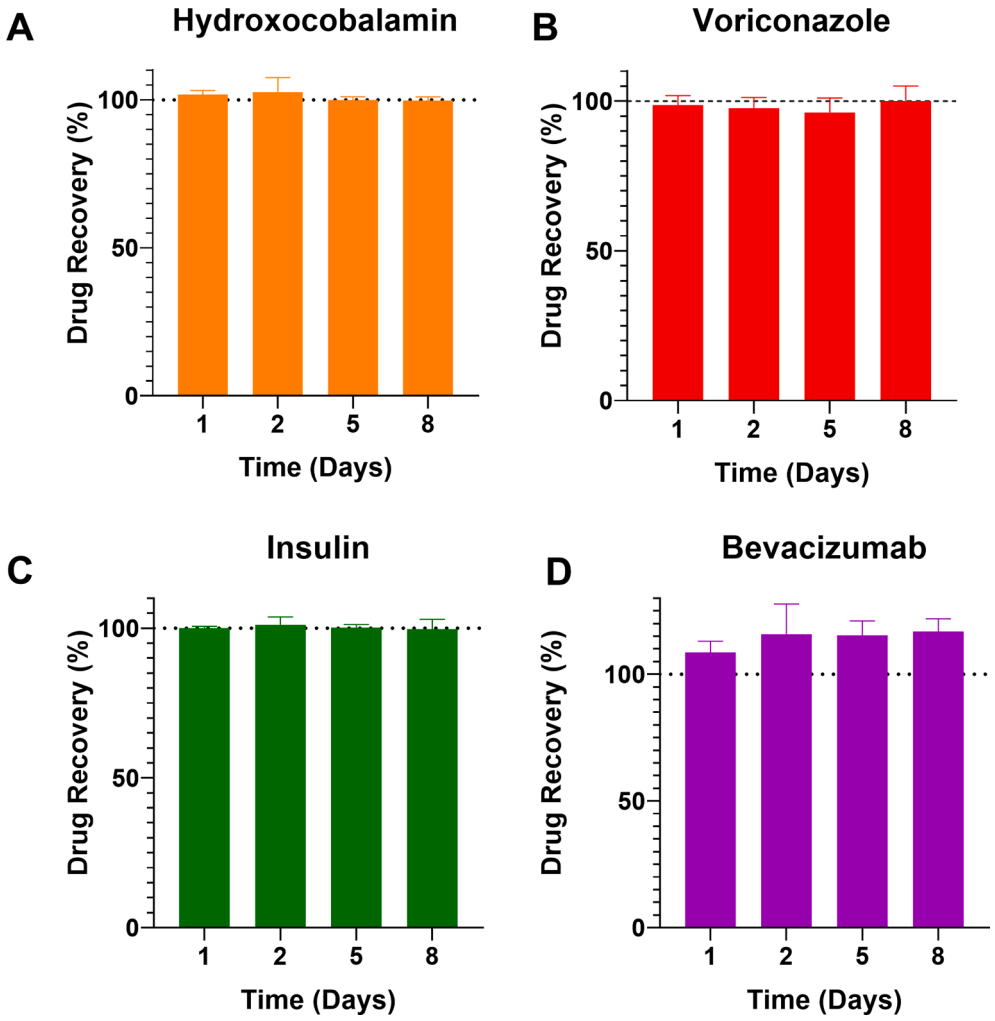

Fig. 4. Drug recovery (%) from 3D printed cylinders coated with coating E compared to glass vials. (A) Hydroxocobalamin acetate recovery (%). (B) Voriconazole recovery (%). (C) Human insulin recovery (%). (D) Bevacizumab recovery (%).

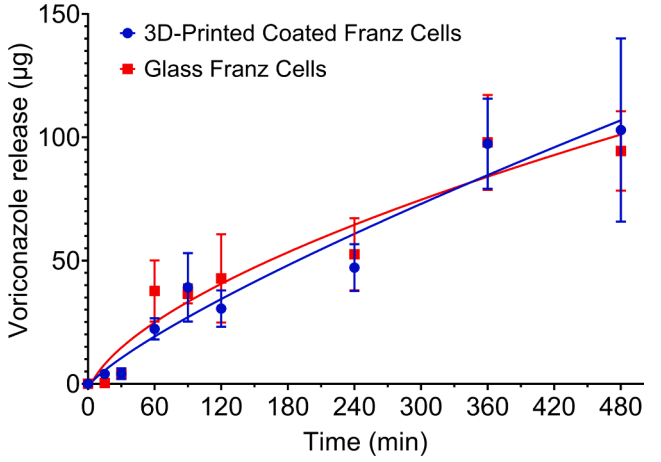

Fig. 5. *In vitro* release of voriconazole eye drops in 3D-printed coated Franz cells and in glass Franz cells (n = 3).

3.4. In vitro release study using voriconazole eye drops in 3D-printed coated Franz cells and glass vertical Franz cells

To compare the suitability of 3D-printed coated Franz cells and conventional glass Franz cells for *in vitro* drug release tests, an *in vitro* release study was performed in triplicate using voriconazole eye drops. The results of the study are shown in Fig. 5. No significant differences were observed in the release of voriconazole from the eye drops between the two types of Franz cells (α n.s.).

Some studies have conducted *in vitro* investigations with different drugs, comparing the drug retention achieved with 3D-printed diffusion cells and conventional glass Franz cells. For instance, in one study, the compatibility of different drugs with 3D-printed diffusion cells using SLA technology was evaluated (Sil et al., 2018). The results revealed the occurrence of drug retention, which was attempted to be addressed by post-processing coating of the devices. However, even with the use of hydrophobic coatings, they proved ineffective in reducing drug retention. In a subsequent study, caffeine was used as a hydrophilic model drug in uncoated SLA 3D-printed devices (Sil et al., 2020). Although the use of this hydrophilic drug improved the compatibility with the SLA acrylic resin, the hydrophobic compounds still did not exhibit compatibility with the proposed model.

In another study, fused deposition modeling (FDM) was used to manufacture vertical diffusion cells using polypropylene (PP) filament (Tiboni et al., 2021). However, it has been shown that PP is susceptible to drug adsorption, thus rendering it unsuitable as an inert material for contact with drug solutions (Palmgrén et al., 2006 Nov 1). On the other hand, polylactic acid (PLA) has also been employed in other studies for 3D printing diffusion cells using FDM technology (Fazili et al., 2020). Nonetheless, PLA exhibits drug adsorption as well (Farto-Vaamonde et al., 2019). In addition, SLA offers certain advantages over FDM

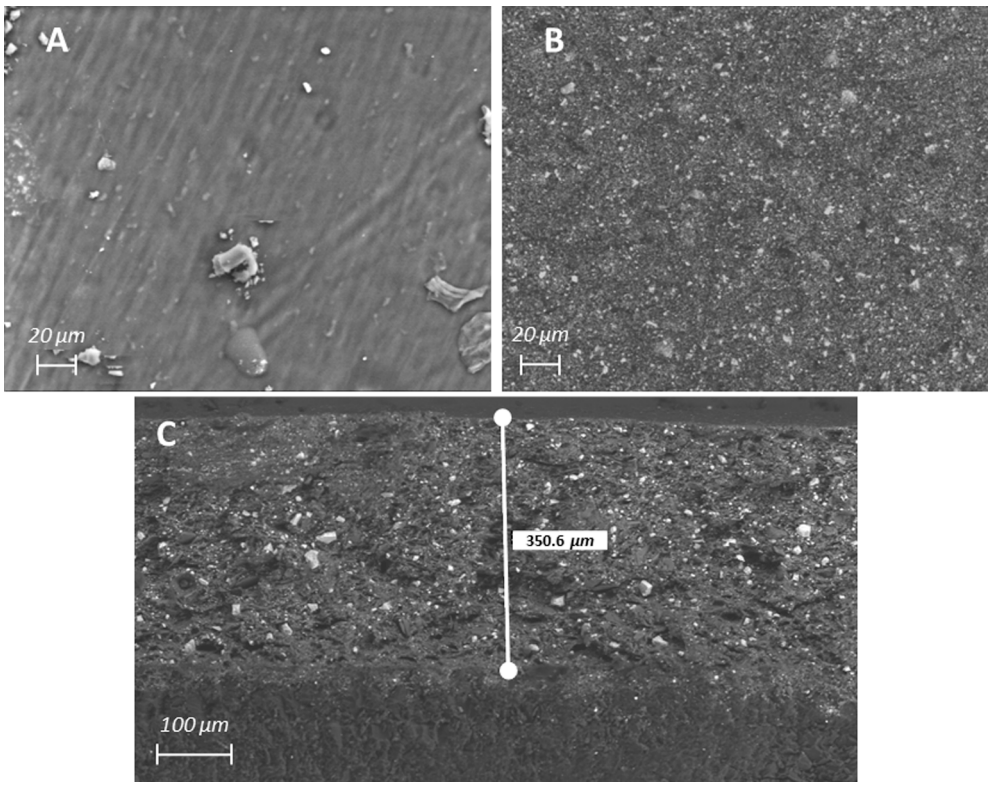

Fig. 6. SEM images of (A) the uncoated resin surface, (B) the coated resin surface, and (C) the side view of the coating E applied to the resin material.

Table 3
Surface elemental analysis of the resin and the coating E.

Element	Resin (%)	Coating E (%)
Carbon (C)	68.4	57.0
Oxygen (O)	31.5	26.8
Titanium (Ti)	–	8.6
Barium (Ba)	–	3.3
Sulphur (S)	–	0.9
Aluminium (Al)	–	0.8
Silicon (Si)	–	0.7
Phosphorus (P)	0.1	0.6
Zinc (Zn)	–	0.6
Magnesium (Mg)	–	0.6
Sodium (Na)	–	0.2

technology. For example, FDM is more prone to production errors and the resulting devices have a higher risk of manufacturing defects (Brion and Pattinson, 2022). In contrast, SLA is significantly and capable of producing several devices simultaneously (Xu et al., 2021; Brion and Pattinson, 2022). FDM filaments typically possess an opaque or slightly translucent nature, whereas SLA resins provide clear and transparent materials (ANYCUBIC 3D Printing [Internet], 2023; Formlabs. [cited 2023 Nov 29]. Guide to Transparent 3D Printing. Available from: https://formlabs.com/blog/3d-printing-transparent-parts-techniques-for-finishing-clear-resin/). Therefore, the coating presented in this study demonstrates more promising outcomes in comparison to those observed in previous studies conducted to date.

3.5. Morphological and physicochemical characterisation of the selected coating

Fig. 6 shows the SEM images of both the uncoated and coated resins surfaces. The uncoated resin surface appears rough and exhibits small fragments of resin adhered to its surface. These resin residues are often deposited during the 3D printing process and their subsequent removal is challenging due to their UV light curing. However, upon the application of coating E, the surface becomes smooth, devoid of significant pores or flaws. The side view of the coated device's surface clearly exhibits the noticeable contrast between the uncoated surface and the E-coated surface. The coating includes small crystals within its composition, a finding confirmed by XRD analysis. The thickness of the coating layer was approximately 350 µm.

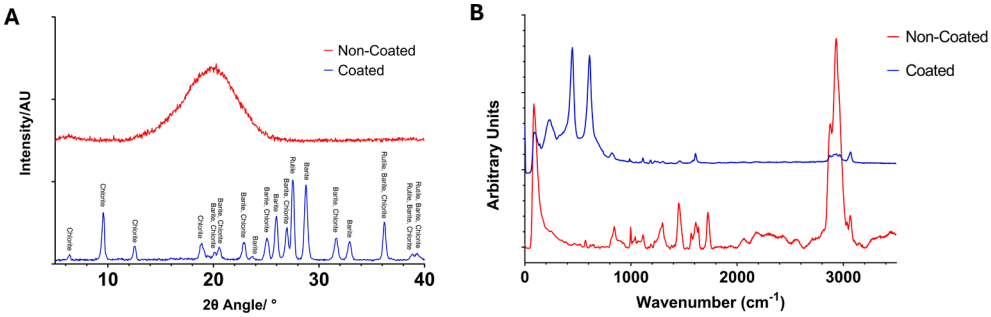

Fig. 7. (A) XRD diffractograms of the surface of coated and uncoated devices (B) Raman spectra of the surface of coated and uncoated devices.

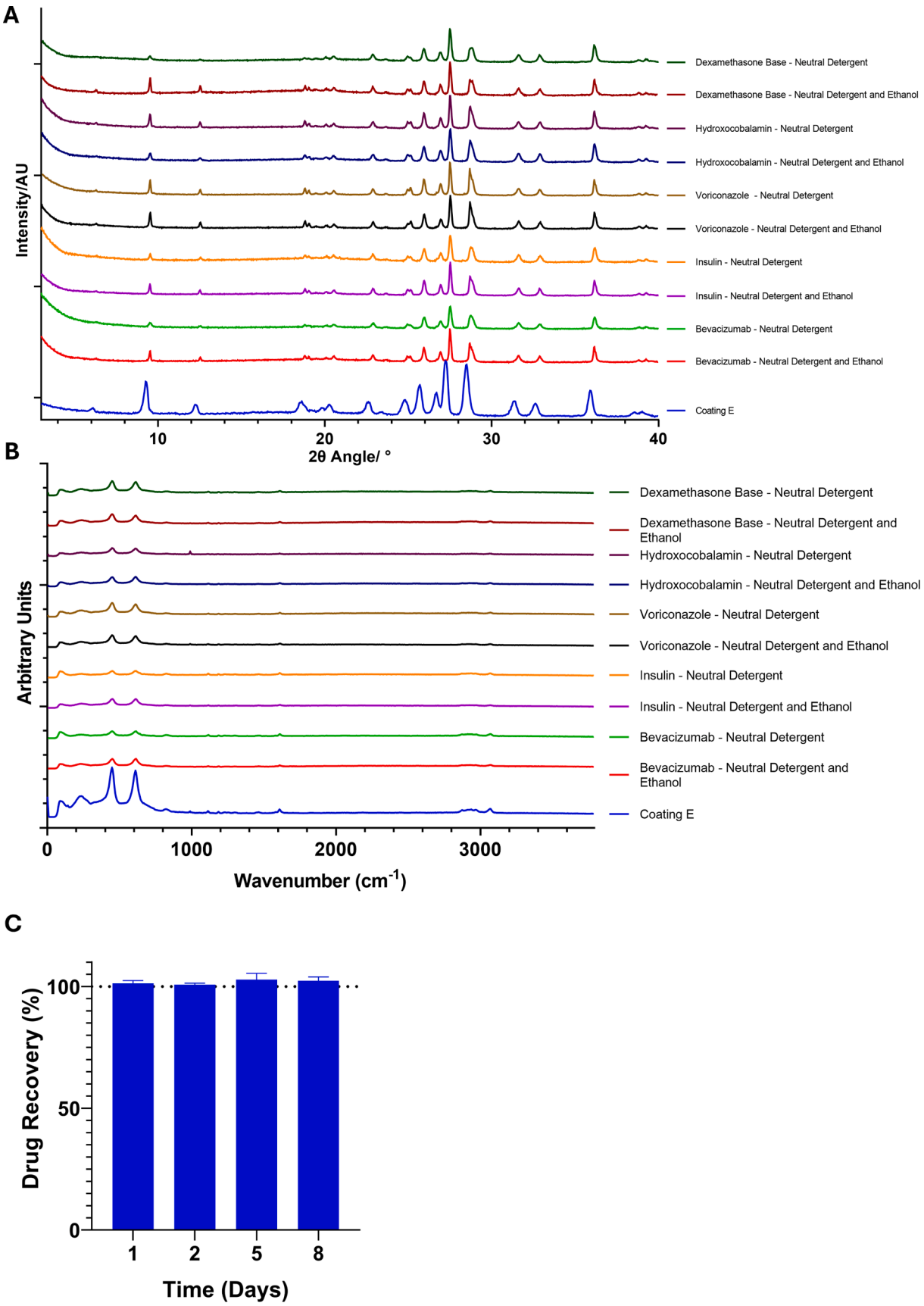

Fig. 8. (A) XRD diffractograms of the washed devices and the coating E (B) Raman spectra of the washed devices and the coating E. (C) Dexamethasone base recovery (%) from recycled 3D printed cylinders coated with coating E.

Table 4
Scherrer's formula results from washed and unwashed coated devices.

Device	Barite crystallite size (nm)	Chlorite crystallite size (nm)	Rutile crystallite size (nm)
Coating E	39.5	40.6	29.7
Bevacizumab – Neutral Detergent	43.4	37.3	50.0
Bevacizumab – Neutral Detergent and Ethanol	77.2	37.8	61.1
Insulin – Neutral Detergent	63.1	35.7	45.7
Insulin – Neutral Detergent and Ethanol	79.4	33.2	59.4
Voriconazole – Neutral Detergent	81.7	83.2	65.3
Voriconazole – Neutral Detergent and Ethanol	77.2	67.0	58.2
Hydroxocobalamin – Neutral Detergent	68.9	72.0	50.9
Hydroxocobalamin – Neutral Detergent and Ethanol	81.7	62.1	61.5
Dexamethasone – Neutral Detergent	46.6	86.6	53.1
Dexamethasone – Neutral Detergent and Ethanol	92.6	86.6	59.8

The surface elemental composition of both the uncoated resin and the coated resin was analysed using EDX. The results of the analysis are presented in Table 3. The acrylic resin primarily consisted of carbon and oxygen, whereas coating E contained a higher proportion of carbon and oxygen, along with trace amounts of titanium, barium, sulphur, aluminium, silicon, phosphorus, zinc, magnesium, and sodium. These findings suggests that coating E incorporates additional components beyond the bisphenol A-based epoxy resin. XRD and Raman analyses were conducted to further investigate the coating E.

Fig. 7**A** shows the XRD diffractogram of the uncoated resin and the coated resin. The resin did not exhibit any diffraction peak as it is in an amorphous state. In contrast, the coated resin, as observed in the SEM images, displayed a micro- or nano-crystalline structure with detectable crystals. The phase identification analysis revealed that the crystalline peaks corresponded to different components, including chlorite (containing Mg, Al, and Si), barite ($BaSO_4$), and rutile (TiO_2), which are essential raw materials in coating and paint industry used to provide resistance, opacity, and colour to the coating. In this case, chlorite was used as a filler and rutile (Pigment White 6 or CI 77891) and barite (Pigment White 21 or CI 77120) were used as white pigments in the coating composition (Völz et al., 2006; Gysau, 2006).

The results of the previous EDX elemental analysis align with the findings from the XRD analysis, as these elements (Mg, Al, Si, Ba, S, Ti, and O) were part of the elemental composition of coating E. It should be noted that these peaks do not indicate the concentration of these compounds in the final composition of coating E, but rather indicate their crystallinity.

Fig. 7**B** presents the Raman spectra of the surface of coated and uncoated devices. Although preforming a comprehensive molecular analysis was challenging due to the complex composition of the resin and coating E, notable variations in the Raman spectra were observed. The Raman spectra of the uncoated device exhibited characteristic features of an acrylic polymer, with a peak at 1715 cm^{-1} corresponding to the C = O bond vibration in the acrylate groups, as well intense peaks in the 2800 – 3000 cm^{-1} region corresponding to C–H bond vibrations of the CH_2 and CH_3 groups of the polymer main chain (De León and Molina, 2020).

On the other hand, the Raman spectra of the coated device displayed weak peaks in the epoxy band (1150–1350 cm^{-1}) at 1257 cm^{-1} and 1186 cm^{-1}, corresponding to the epoxy ring breathing vibration and the C-O-C backbone vibration, respectively (Lyon et al., 1994). The intense peaks observed at 448 cm^{-1} and 612 cm^{-1} are associated to O-Ti bonds from the TiO_2 used as an opacifier in the coating composition, as confirmed by the EDX and XRD results (Balachandran and Eror, 1982).

Based on the Raman results, it was observed that the coating was uniformly applied to the resin surface. The components of the coating did not react with those of the resin. Additionally, only the spectrum of coating E was detected in the analysed area, indicating the absence of pores that could expose the resin to contact with the drug. These results suggest that the coating E could be used with different types of resin or 3D printing materials.

3.6. Evaluation of the reusability of the coated devices

The 3D-printed cylinders coated with coating E were cleansed using a neutral detergent or a combination of neutral detergent and alcohol. An EDX analysis was performed to detect any potential changes in the elemental composition of the coating that could have resulted from drug retention during contact. The analysis focused on identifying atoms specific to the drugs that had come into contact with the coating, including nitrogen (ciclopirox olamine, bevacizumab, human insulin, and voriconazole), cobalt (hydroxocobalamin), and fluorine

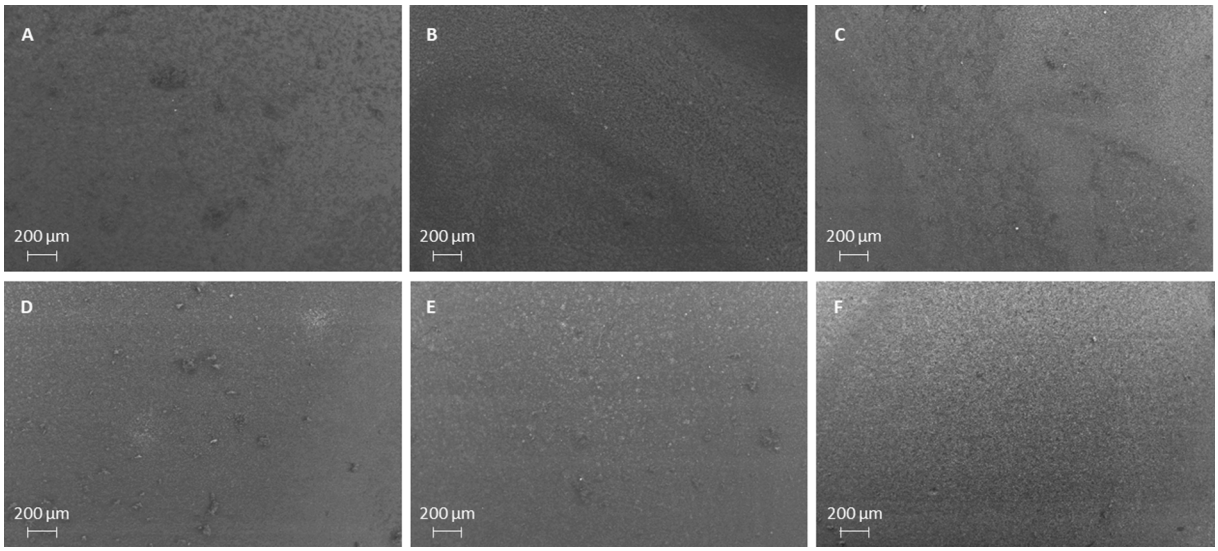

Fig. 9. SEM images of the coating surface after exposure to (A) liquid paraffine, (B) acetone, (C) ethanol, (D) isopropanol, (E) neutral detergent, (F) methanol.

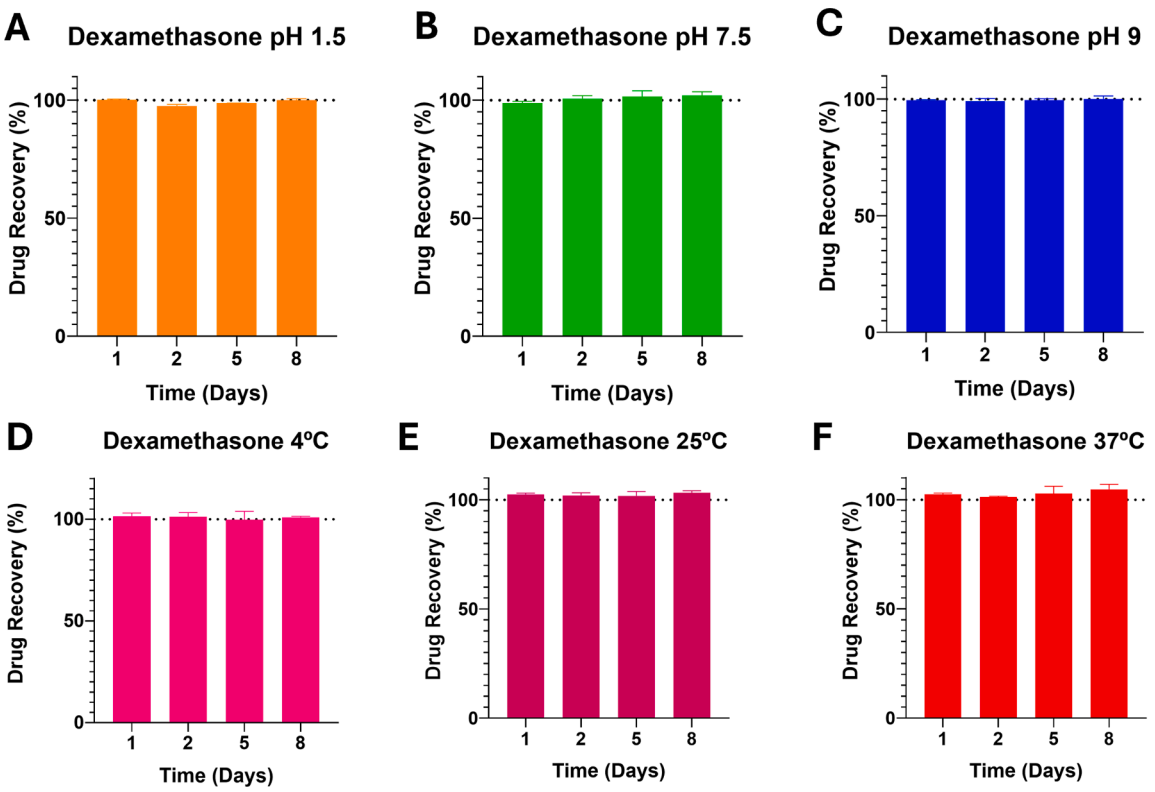

Fig. 10. (A, B, C) Recovery (%) of dexamethasone base at different temperature values (D, E, F) Recovery (%) of dexamethasone base after exposure of coating E to buffers of different pH's.

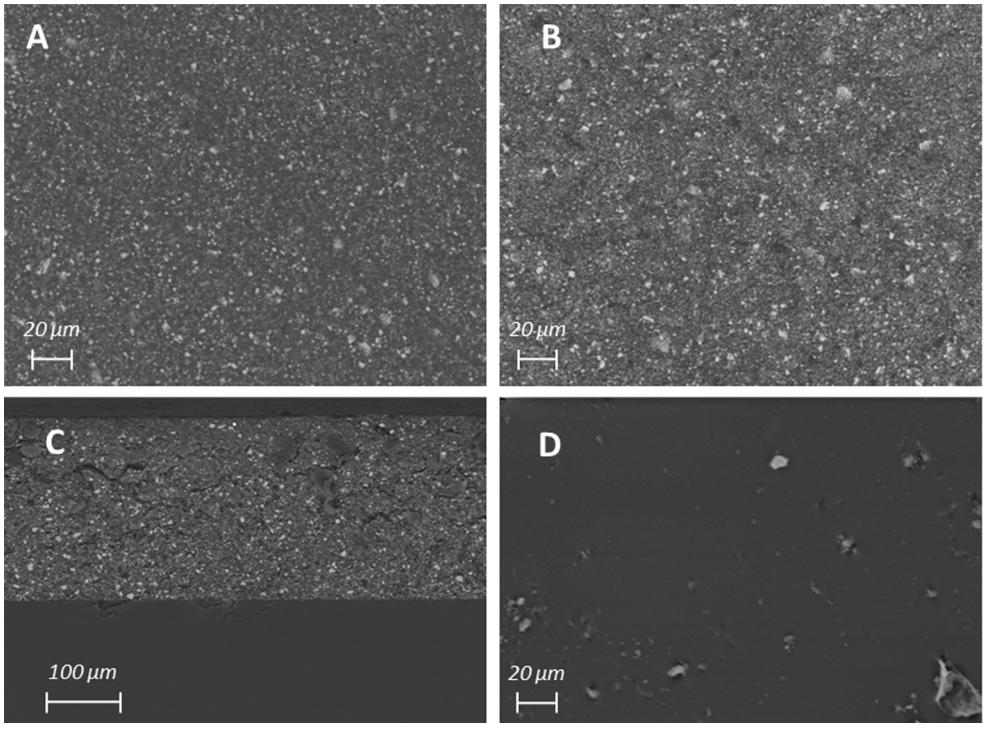

Fig. 11. SEM images of (A) coating F, (B) coating E, (C) the side view of the coating F applied to the resin material, (D) coating G.

(dexamethasone base and voriconazole). The EDX analysis did not detect the presence of any target atoms, indicating that the drugs did not adhere to the coating's surface. Furthermore, there were no significant differences in composition between the unwashed devices, those washed with neutral detergent, and those that were washed with neutral detergent and alcohol.

A XRD analysis was performed to examine potential changes in the coating's crystallinity after washing and to detect any peaks

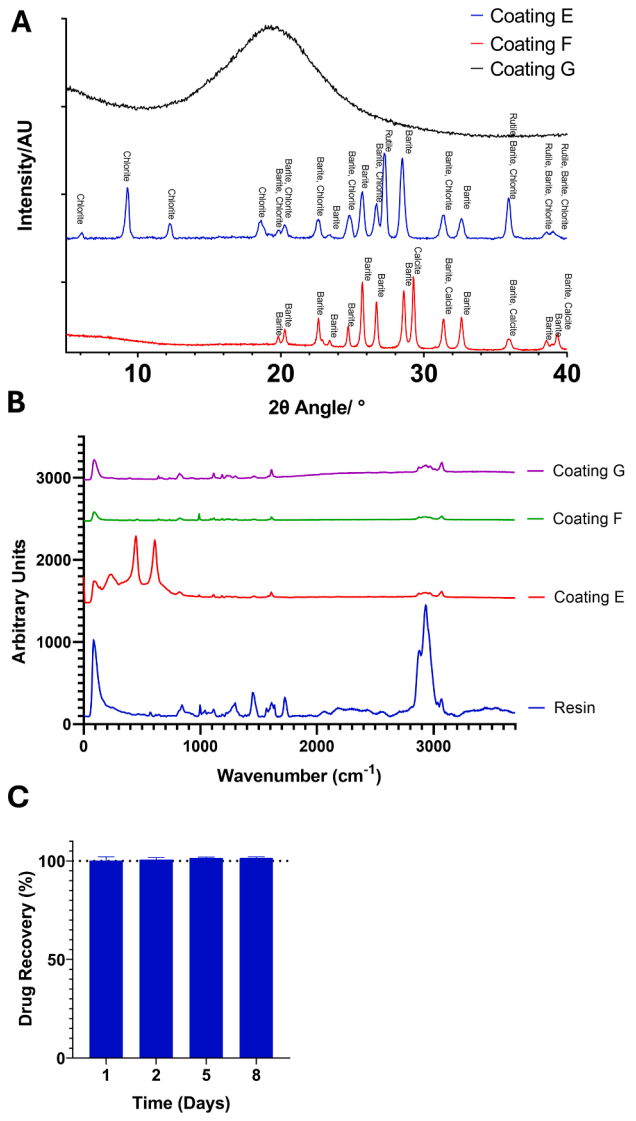

Fig. 12. (A) XRD diffractogram of the surface of coating E and coating F (B) Raman spectra of the surface of coating E and coating F (C) Dexamethasone base recovery (%) from 3D-printed cylinders coated with coating F.

Table 5
Elemental analysis of the surface of coating E, F, and G.

Element	Coating E (%)	Coating F (%)	Coating G (%)
Carbon (C)	57.0	66.1	81.2
Oxygen (O)	26.8	18.9	18.5
Titanium (Ti)	8.6	–	–
Barium (Ba)	3.3	7.4	–
Sulphur (S)	0.9	1.8	–
Aluminium (Al)	0.8	<0.1	–
Silicon (Si)	0.7	<0.1	–
Phosphorus (P)	0.6	<0.1	0.2
Zinc (Zn)	0.6	–	–
Magnesium (Mg)	0.6	0.1	–
Sodium (Na)	0.2	<0.1	–
Calcium (Ca)	–	5.2	–
Chloride (Cl)	–	–	0.1

corresponding to drug crystallisation. Fig. 8**A** shows the diffractograms of all the tested devices. All observed peaks corresponded to the coating matrix, which confirms the absence of drug retention within the coating. While there were variations in the crystallinity of the phases after cleansing, all phases remained present. A slight broadening of the peaks was observed after washing, suggesting a minor increase in crystallinity.

The Scherrer's formula was employed to assess the change in coating crystallinity before and after washing. The crystallite sizes of barite, chlorite and rutile were determined (Table 4) and compared across the different devices. The washed coated devices exhibited larger crystallite domain sizes for all components, regardless of the washing method ($\alpha < 0.05$). Some components of coating E may have dissolved during washing with water or ethanol. During the drying process, these compounds could crystallise, leading to the formation of larger crystals with different conformations.

Raman spectroscopy analysis was performed to assess potential changes in the functional groups present on the surface of the washed coated devices. Fig. 8**B** shows the Raman spectra of the washed devices compared to coating E. The peaks associated with Ti-O bonds exhibited reduced intensity in the washed devices, suggesting that the cleaning process or the previous incubation experiment might remove some TiO_2 particles from the surface of the coating. Moreover, the XRD results suggested an increase in rutile crystallite size. Consequently, the analysed area may possess larger crystals, albeit in lesser quantity than before washing, which could explain the diminished intensity of the Ti-O bonds peaks. However, no new peaks were observed in the Raman analysis for any of the drugs, indicating that coating E did not cause drug retention.

The recycled 3D-printed coated cylinders underwent drug retention testing by introducing a 25 μg/mL solution of dexamethasone base after cleansing and drying. Fig. 8**C** illustrates that the recycled devices exhibited complete recovery of dexamethasone base, with no drug retention observed at any time point. No significant differences were found between time points for dexamethasone base (α n.s.). These results demonstrate that the coated devices are reusable, since the cleaning process did not impact drug retention.

3.7. Solvent resistance of the selected coating

The coated cylinders were exposed to a variety of commonly used solvents, including liquid paraffin, acetone, ethanol, isopropanol, neutral detergent, and methanol. SEM images of the cylinders after exposure to the solvents are shown in Fig. 9. Prior to exposure, the solvents were visually examined for any signs of turbidity, and no visual disturbances were observed after contact with the coating. SEM images were inspected to identify possible changes in the morphology of the coating surface, such as pores or imperfections, but no significant alterations were observed for any of the solvents. These results indicate that coating E is compatible with the tested solvents.

3.8. Temperature and pH resistance

A dexamethasone base retention test was performed to assess the thermal stability of the coated devices. The temperatures tested were 4 °C, 25 °C, and 37 °C. A 25 μg/mL dexamethasone base solution was added to the devices to assess drug retention. On day 8, the recovery of the dexamethasone base was approximately 100 % for all tested temperatures, except for 37 °C, where recovery was 104.72 ± 2.31 % (Fig. 10**A, B, C**). This slight increase in recovery at 37 °C was likely due to evaporation of the solvent in the 3D-printed cylinders, which were covered with Parafilm® M sealing film instead of a cap like the glass vials.

Although the previously tested drug solutions (Section 2.4 and 2.6) covered a wide range of pH levels, a specific test was carried out to investigate the potential influence of pH on drug retention. The coated devices were filled with various buffers of different pH's (pH 1.2, 7.5 and 9). After 24 h, the buffers were removed, and a drug retention test was performed using a 25 μg/mL dexamethasone base solution. The coated devices showed complete recovery of dexamethasone base with no significant drug retention at all time points (α n.s.) (Fig. 10**D, E, F**). On day

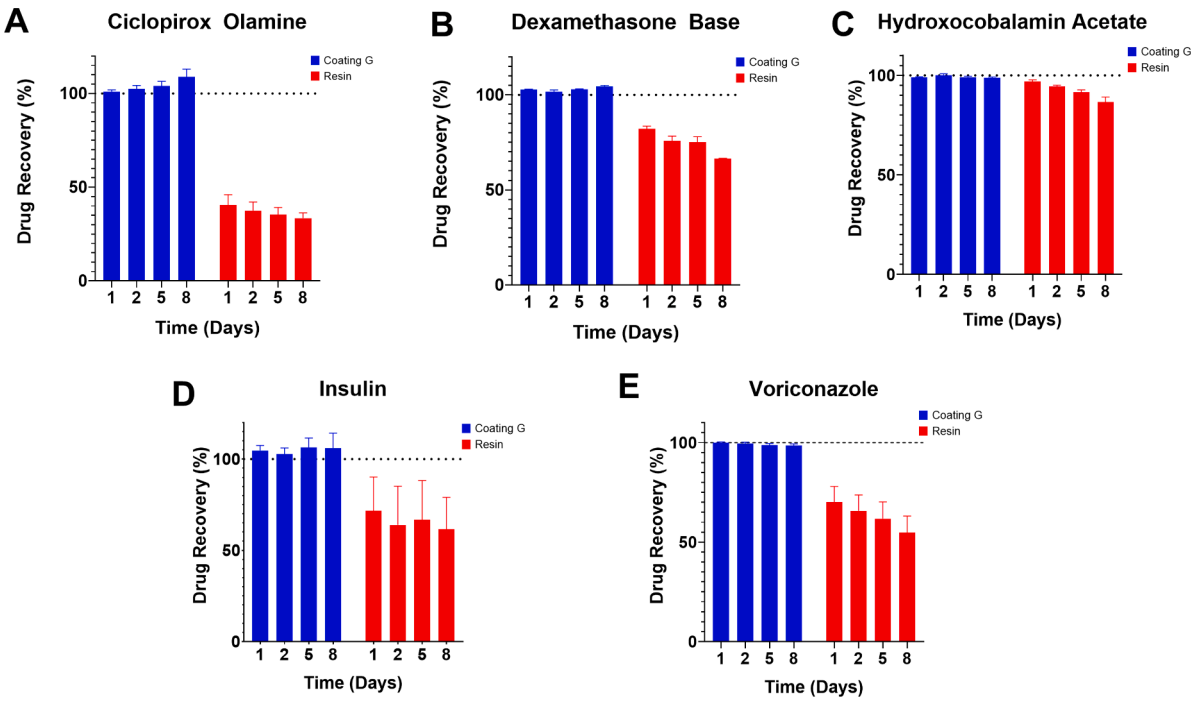

Fig. 13. Drug recovery (%) from 3D printed cylinders coated with coating G and non-coated cylinders compared to glass vials.

8, the recovery of the dexamethasone base was approximately 100 % for all pH values tested.

3.9. Comparison between the opaque coating (E), the translucent coating (F), and the in-house made coating (G)

The microscopic appearance of the surface of coatings F and G is shown in Fig. 11. As with coating E, no large pores or defects were observed. This indicates that the coatings F and G cover the entire surface of the resin. Small crystals are visible on the surface of the coating F, the presence of which was confirmed by XRD analysis (Fig. 12**A**).

The elemental composition of the surface of coatings F and G was analysed by EDX and compared with that of coating E. Table 5 presents the comparison of the elemental composition between coating E, F, and G. Coating G is primarily composed of C and O, aligning with its expected composition. Coating E includes Ti from rutile molecules, serving as a white pigment. Moreover, coating E contains chlorite, incorporating Mg, Al, and Si elements. Coating F, on the other hand, shows a lower proportion of these elements, suggesting the absence of chlorite. The presence of Ba suggests that barite is present in both coatings, although it appears to be in a higher proportion in the coating F.

Coating F also contains calcium (Ca). To determine to which compound the calcium belongs to, an XRD analysis was performed. Fig. 12**A** shows the diffractograms of coatings E, F, and G. The previously analysed Ca corresponds to calcium carbonate or calcite ($CaCO_3$) molecules, probably included to act as filler material to provide hardness and flexibility to the coating polymer (Gysau, 2006). As can be seen, the peaks corresponding to rutile are not visible, demonstrating that rutile is not part of the composition of Coating F. Coating G shows an XRD pattern characteristic of an amorphous state due to its polymeric composition.

The Raman spectra confirmed the absence of TiO_2 in the coating F, since the peaks corresponding to the Ti-O bonds were missing (Fig. 12**B**). Despite this difference, the spectra of both coatings were similar, suggesting a similar composition. Similarly, coating G showed only the characteristic peaks of the polymer. Notably, the Raman spectra did not reveal any peaks associated with the acrylic resin beneath the coating, emphasising the effectiveness of the coating process.

Coating F was tested for dexamethasone base retention by introducing a 25 μg/mL solution into F-coated 3D-printed cylinders. Fig. 12**C** shows that coating F exhibited complete recovery of dexamethasone base with no drug retention at all time points, with no significant difference between time points being found for dexamethasone base (α n. s.). In addition, no significant differences were found between dexamethasone base retention in coating E and F (α n.s.). These results suggest that coating F would not cause drug retention, although further studies with more types of drugs are required.

Coating G was tested for drug retention by introducing 100 μg/mL human insulin, 25 μg/mL dexamethasone base, 50 μg/mL voriconazole with 0.1 % (w/v) 2-hydroxypropyl-β-cyclodextrin (HPβCD), 50 μg/mL hydroxocobalamin acetate, and 50 μg/mL ciclopirox olamine solutions into G-coated 3D-printed cylinders. Fig. 13 shows that coating G exhibited complete recovery of all the drugs, with no drug retention at any time point.

4. Conclusion

For the first time, the development of an inert coating specifically designed for 3D printed diffusion models has been achieved. This coating effectively prevents drug retention during *in vitro* drug release studies, encompassing small molecules as well as biologics from pharmaceutical formulations. The application of this coating to the 3D-printed models ensured their leak-free performance and demonstrated excellent chemical resistance to solvents. Furthermore, the coating's opacity renders these 3D models highly suitable for light-sensitive drugs. Leveraging the versatility of 3D printing, these models can be tailored to accommodate formulations intended for various routes of administration, providing adaptability in terms of geometries and volumes. Ultimately, the coatings presented in this study will facilitate the integration of 3D-printed diffusion models into pre-formulation pharmaceutical studies, paving the way for the use of sustainable and reusable devices that are both robust and cost-effective to produce.

A patent has been applied to protect the application of these coatings (Method of manufacture of a laboratory object suitable for experiments with active pharmaceutical or cosmetic active (ES202331049), 2023.).

CRediT authorship contribution statement

Carlos Bendicho-Lavilla: Writing – review & editing, Writing – original draft, Visualization, Validation, Supervision, Software, Resources, Project administration, Methodology, Investigation, Formal analysis, Data curation, Conceptualization. **Victoria Díaz-Tomé:** Writing – review & editing, Writing – original draft, Visualization, Validation, Supervision, Software, Resources, Project administration, Methodology, Investigation, Formal analysis, Data curation, Conceptualization. **Iria Seoane-Viaño:** Writing – review & editing, Writing – original draft. **Asteria M. Luzardo-Álvarez:** Writing – review & editing. **Francisco J. Otero-Espinar:** Writing – review & editing, Writing – original draft, Visualization, Validation, Supervision, Software, Resources, Project administration, Methodology, Investigation, Funding acquisition, Formal analysis, Data curation, Conceptualization.

Declaration of competing interest

The authors declare that they have no known competing financial interests or personal relationships that could have appeared to influence the work reported in this paper.

Data availability

Data will be made available on request.

Acknowledgements

I.S.V. and V. D. T acknowledges Consellería de Cultura, Educación e Universidade for their Postdoctoral Fellowships (Xunta de Galicia, Spain; ED481B-2021-019 and ED481B-2023-092). Work supported by MICINN [PID2022-142350OB-C21]. Authors would like to thank the use of RIAIDT-USC analytical facilities. In addition, the authors would like to acknowledge Diego Romero López for the resources provided.

REFERENCES

ANYCUBIC 3D Printing [Internet]. [cited 2023 Mar 29]. Colored UV Resin 1KG. Available from: https://www.anycubic.com/products/colored-uv-resin-for-photon-series.

Auel, T., Großmann, L., Schulig, L., Weitschies, W., Seidlitz, A., 2021 Sep. The EyeFlowCell: Development of a 3D-Printed Dissolution Test Setup for Intravitreal Dosage Forms. Pharmaceutics. 13 (9), 1394.

Balachandran, U., Eror, N.G., 1982. Raman spectra of titanium dioxide. J. Solid State Chem. 42 (3), 276–282.

Bendicho-Lavilla, C., Seoane-Viaño, I., Otero-Espinar, F.J., Luzardo-Álvarez, A., 2022 Feb. Fighting type 2 diabetes: Formulation strategies for peptide-based therapeutics. Acta Pharm Sin B. 12 (2), 621–636.

Bendicho-Lavilla, C., Seoane-Viaño, I., Santos-Rosales, V., Díaz-Tomé, V., Carracedo-Pérez, M., Luzardo-Álvarez, A.M., et al., 2023 Oct. Intravitreal implants manufactured by supercritical foaming for treating retinal diseases. J. Control. Release 1 (362), 342–355.

Benmessaoud, N., Hamri, S., Bouchaour, T., Maschke, U., 2020. Swelling and thermal behavior of a cross-linked polymer networks poly(2-phenoxyethyl acrylate): exploitation by the Voigt viscoelastic model. Polym Bull. 77 (10), 5567–5588.

Bown, H.K., Bonn, C., Yohe, S., Yadav, D.B., Patapoff, T.W., Daugherty, A., et al., 2018 Mar. In vitro model for predicting bioavailability of subcutaneously injected monoclonal antibodies. J Control Release. 10 (273), 13–20.

Brion, D.A.J., Pattinson, S.W., 2022 Aug 15. Generalisable 3D printing error detection and correction via multi-head neural networks. Nat Commun. 13 (1), 4654.

Anycubic Resin Printer - Anycubic. [cited 2023 Nov 18]. Available from: https://www.anycubic.es/.

Center for Drug Evaluation and Research. U.S. Food and Drug Administration. FDA; 2020 [cited 2023 Jun 1]. SUPAC-SS: Nonsterile Semisolid Dosage Forms; Scale-Up and Post-Approval Changes: Chemistry, Manufacturing and Controls; In Vitro Release Testing and In Vivo Bioequivalence Documentation. Available from: https://www.fda.gov/regulatory-information/search-fda-guidance-documents/supac-ss-nonsterile-semisolid-dosage-forms-scale-and-post-approval-changes-chemistry-manufacturing.

Center for Drug Evaluation and Research. U.S. Food and Drug Administration. FDA; 2022 [cited 2023 Jun 1]. In Vitro Permeation Test Studies for Topical Drug Products Submitted in ANDAs. Available from: https://www.fda.gov/regulatory-information/search-fda-guidance-documents/in-vitro-permeation-test-studies-topical-drug-products-submitted-andas.

Council of Europe. 4.1.3. Buffer Solutions. In: European Pharmacopoeia. 7th ed. Strasbourg: Council of Europe; p. 489–94.

De León, A.S., Molina, S.I., 2020 May. Influence of the Degree of Cure in the Bulk Properties of Graphite Nanoplatelets Nanocomposites Printed via Stereolithography. Polymers 12 (5), 1103.

Díaz-Tomé, V., García-Otero, X., Varela-Fernández, R., Martín-Pastor, M., Conde-Penedo, A., Aguiar, P., et al., 2021 Mar. In situ forming and mucoadhesive ophthalmic voriconazole/HPβCD hydrogels for the treatment of fungal keratitis. Int. J. Pharm. 15 (597), 120318.

Creality Resin Printer - Creality. [cited 2023 Nov 18]. Available from: https://www.creality3dofficial.com/collections/lcd-uv-resin-3d-printer.

Farto-Vaamonde, X., Auriemma, G., Aquino, R.P., Concheiro, A., Alvarez-Lorenzo, C., 2019 Aug. Post-manufacture loading of filaments and 3D printed PLA scaffolds with prednisolone and dexamethasone for tissue regeneration applications. Eur. J. Pharm. Biopharm. 1 (141), 100–110.

Fazili, Z., Ward, A., Walton, K., Blunt, L., Asare-Addo, K., 2020. Design and development of a novel fused filament fabrication (FFF) 3D printed diffusion cell with UV imaging capabilities to characterise permeation in pharmaceutical formulations. Eur. J. Pharm. Biopharm. 1 (152), 202–209.

ELEGOO Resin Printer - ELEGOO. [cited 2023 Nov 18]. Available from: https://www.elegoo.com/pages/elegoo-bf2022?gclid=Cj0KCQiA99ybBhD9ARIsALvZavXU5pZ1yPOz2g3Lb6ajr97MJ1cG6k7G_7bHAyeBqtJJf-tm-J_VqcYaArVTEALw_wcB.

García-Otero, X., Mondelo-García, C., Bandín-Vilar, E., Gómez-Lado, N., Silva-Rodríguez, J., Rey-Bretal, D., et al., 2022 Nov. PET study of intravitreal adalimumab pharmacokinetics in a uveitis rat model. Int. J. Pharm. 5 (627), 122261.

Ghosh, P., Milewski, M., Paudel, K., 2015. In vitro/in vivo correlations in transdermal product development. Ther Deliv. 6 (9), 1117–1124.

Gysau, D., 2006. Fillers for Paints: Fundamentals and Applications. Vincentz Network GmbH & Co KG 30, p.

Hoehne, M., Samuel, F., Dong, A., Wurth, C., Mahler, H.C., Carpenter, J.F., et al., 2011. Adsorption of monoclonal antibodies to glass microparticles. J. Pharm. Sci. 100 (1), 123–132.

Kinnunen, H.M., Sharma, V., Contreras-Rojas, L.R., Yu, Y., Alleman, C., Sreedhara, A., et al., 2015 Sep. A novel in vitro method to model the fate of subcutaneously administered biopharmaceuticals and associated formulation components. J. Control Release. 28 (214), 94–102.

Lyon, R.E., Chike, K.E., Angel, S.M., 1994. In situ cure monitoring of epoxy resins using fiber-optic Raman spectroscopy. J. Appl. Polym. Sci. 53 (13), 1805–1812.

Malinowski, H., Marroum, P., Uppoor, V.R., Gillespie, W., Ahn, H.Y., Lockwood, P., et al., 1997. Draft guidance for industry extended-release solid oral dosage forms. Development, evaluation and application of in vitro-in vivo correlations. Adv. Experim. Med. Biol. 423, 269–288.

Formlabs. [cited 2023 Nov 29]. Guide to Transparent 3D Printing. Available from: https://formlabs.com/blog/3d-printing-transparent-parts-techniques-for-finishing-clear-resin/.

Method of manufacture of a laboratory object suitable for experiments with active pharmaceutical or cosmetic active (2023), Patent application ES202331049.

Mohmmed, S.A., Vianna, M.E., Hilton, S.T., Boniface, D.R., Ng, Y.L., Knowles, J.C., 2017. Investigation to test potential stereolithography materials for development of an in vitro root canal model. Microsc. Res. Tech. 80 (2), 202–210.

Palmgrén, J.J., Mönkkönen, J., Korjamo, T., Hassinen, A., Auriola, S., 2006 Nov 1. Drug adsorption to plastic containers and retention of drugs in cultured cells under in vitro conditions. Eur. J. Pharm. Biopharm. 64 (3), 369–378.

Phan, C.M., Shukla, M., Walther, H., Heynen, M., Suh, D., Jones, L., 2021 Feb 25. Development of an in vitro blink model for ophthalmic drug delivery. Pharmaceutics. 13 (3), 300.

PermeGear. Diffusion Cell Basics . [cited 2022 Oct 31]. Available from: https://permegear.com/wp-content/uploads/2019/11/Diffusion-Cell-Basics.pdf.

PermeGear. Diffusion Testing Fundamentals. [cited 2022 Oct 31]. Available from: https://permegear.com/wp-content/uploads/2015/08/primer.pdf.

Rodríguez-Pombo, L., Xu, X., Seijo-Rabina, A., Ong, J.J., Alvarez-Lorenzo, C., Rial, C., et al., 2022 Apr. Volumetric 3D printing for rapid production of medicines. Addit. Manuf. 1 (52), 102673.

Salamanca, C.H., Barrera-Ocampo, A., Lasso, J.C., Camacho, N., Yarce, C.J., 2018 Sep 5. Franz diffusion cell approach for pre-formulation characterisation of ketoprofen semi-solid dosage forms. Pharmaceutics. 10 (3), 148.

Seoane-Viaño, I., Gómez-Lado, N., Lázare-Iglesias, H., Rey-Bretal, D., Lamela-Gómez, I., Otero-Espinar, F., et al., 2019 Oct. Evaluation of the therapeutic activity of Melatonin and Resveratrol in Inflammatory Bowel Disease: a longitudinal PET/CT study in an animal model. Int. J. Pharm. 5, 118713.

Seoane-Viaño, I., Otero-Espinar, F.J., Goyanes, Á., 2021. 3D printing of pharmaceutical products. Addit. Manuf. 569–597.

Seoane-Viaño, I., Ong, J.J., Basit, A.W., Goyanes, A., 2022 Dec. To infinity and beyond: Strategies for fabricating medicines in outer space. Int. J. Pharm. X. 1 (4), 100121.

Sil, B.C., Alvarez, M.P., Zhang, Y., Kung, C.P., Hossain, M., Iliopoulos, F., et al., 2018 Dec. 3D-printed Franz type diffusion cells. Int. J. Cosmet. Sci. 40 (6), 604–609.

Sil, B.C., Belgrave, R.G., Alvarez, M.P., Luo, L., Cristofoli, M., Penny, M.R., et al., 2020. 3D-Printed Franz cells – update on optimization of manufacture and evaluation. Int. J. Cosmet. Sci. 42 (4), 415–419.

PubChem. [cited 2023 Sep 22]. Available from: https://pubchem.ncbi.nlm.nih.gov/.

Fisher Scientific. Franz Cell. [cited 2022 Oct 31]. Available from: https://www.fishersci.com/us/en/catalog/search/products?keyword=franz+cell.

Tiboni, M., Curzi, G., Aluigi, A., Casettari, L., 2021 Oct. An easy 3D printing approach to manufacture vertical diffusion cells for in vitro release and permeation studies. J. Drug Delivery Sci. Technol. 1 (65), 102661.

Voet, V.S.D., Strating, T., Schnelting, G.H.M., Dijkstra, P., Tietema, M., Xu, J., et al., 2018 Feb 28. Biobased acrylate photocurable resin formulation for stereolithography 3D printing. ACS Omega 3 (2), 1403–1408.

NC3Rs. [cited 2023 Mar 2]. Available from: https://nc3rs.org.uk/who-we-are/3rs.

Völz HG, Kischkewitz J, Woditsch P, Westerhaus A, Griebler WD, De Liedekerke M, et al. Pigments, Inorganic. In: Ullmann's Encyclopedia of Industrial Chemistry. John Wiley & Sons, Ltd; 2006 [cited 2023 Sep 18]. Available from: https://onlinelibrary.wiley.com/doi/abs/10.1002/14356007.a20_243.pub2.

Wei, Q., Becherer, T., Angioletti-Uberti, S., Dzubiella, J., Wischke, C., Neffe, A.T., et al., 2014. Protein interactions with polymer coatings and biomaterials. Angew. Chem. Int. Ed. 53 (31), 8004–8031.

Xu, X., Awad, A., Robles-Martinez, P., Gaisford, S., Goyanes, A., Basit, A.W., 2021 Jan. Vat photopolymerization 3D printing for advanced drug delivery and medical device applications. J. Control. Release 10 (329), 743–757.